LAPP-EXP-95-08

The NOMAD Experiment at the CERN SPS

Elena Manola-Poggioli

Laboratoire d'Annecy-le-Vieux de Physique des Particules
Chemin de Bellevue, B.P.110
74941 ANNECY-LE-VIEUX CEDEX FRANCE

Abstract

The NOMAD experiment is searching for the ν_τ appearence in the CERN wide-band neutrino beam. The experiment is sensitive to the oscillations $\nu_\tau - \nu_\mu$ having the mixing angle greater than $sin^2(2\Theta) = 3.8 \times 10^{-4}$, for the mass difference squared $\Delta m^2 > 0.7 eV^2$. If no oscillation events are seen, the existing experimental limits would improve by one order of magnitude in the cosmologically prefered ν_τ mass region. The ν_τ signal will be searched for using the kinematical criteria only.The completed NOMAD detector is currently collecting data.

Talk given at the Four Seas Conference
June 25 - July 1, 1995
Trieste, Italy

The NOMAD Experiment at the CERN SPS

Elena Manola-Poggioli
Laboratoire d'Annecy-le-Vieux de Physique des Particules
Chemin de Bellevue, B.P.110
74941 ANNECY-LE-VIEUX CEDEX FRANCE
On behalf of the NOMAD Collaboration

ABSTRACT

The NOMAD experiment is searching for the ν_τ appearence in the CERN wide-band neutrino beam. The experiment is sensitive to the oscillations $\nu_\tau - \nu_\mu$ having the mixing angle greater than $sin^2(2\Theta) = 3.8 \times 10^{-4}$, for the mass difference squared $\Delta m^2 > 0.7eV^2$. If no oscillation events are seen, the existing experimental limits would improve by one order of magnitude in the cosmologically prefered ν_τ mass region. The ν_τ signal will be searched for using the kinematical criteria only. The completed NOMAD detector is currently collecting data.

1 Introduction

The main goal of the NOMAD (Neutrino Oscillation MAgnetic Detector) experiment [1] at CERN is to search for the $\nu_\mu - \nu_\tau$ oscillations in the SPS wide band neutrino beam. The ν_μ beam has a mean energy of 27 GeV and contains about 1% of ν_e. The contamination of the prompt ν_τ from Ds mesons decays is negligible (10^{-7}). For the accumulated SPS intensity of 2.4×10^{19} protons-on-target (p.o.t.), which corresponds to 2 years of run, NOMAD should observe about 1.5×10^6 neutrino interactions in the fiducial volume.

In the 2-families mixing scenario, the neutrino oscillations are parametrized by a mass difference squared Δm^2 and a mixing angle $sin^2\Theta$. The probability of observing neutrino oscillations at the distance L from the production point is given by $P(L) = sin^2(2\Theta) \times sin^2(\pi L/L_{osc})$ where $L_{osc} = (4\pi E)/\Delta m^2$. The region of the neutrino masses an experiment is suited to probe will be determined by the ratio E/L, while limits on $sin^2(2\Theta)$ depend on the accumulated statistics. Being located at the SPS West Area together with CHORUS [2], about 820 m from the production target , NOMAD experiment is sensitive on the neutrino oscillations with $\Delta m^2 > 0.7eV^2$ that corresponds to maximal mixing (Fig. 1). The best sensitivity of NOMAD for the $\nu_\mu - \nu_\tau$ oscillations is obtained for the $\Delta m^2 > 20eV^2$, where the experiment is capable of detecting oscillations if the mixing strenght is greater than 1.9×10^{-4} (90%CL). If the oscillation events are not found, NOMAD will improve the current best limit from E531 [4] experiment by one order of magnitude.

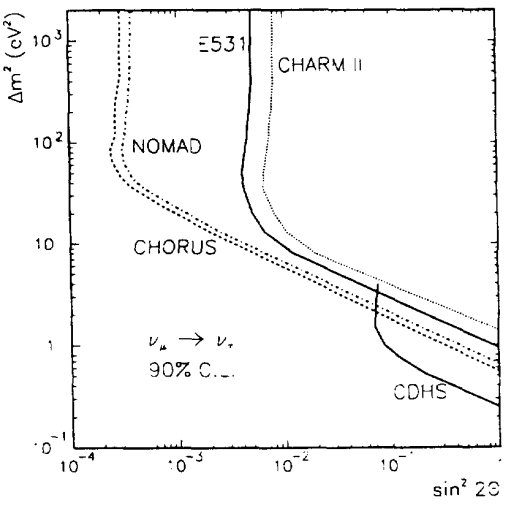

Figure 1: *$\nu_\mu - \nu_\tau$ oscillation parameter exclusion regions at 90% CL.*

2 Analysis method

The ν_τ is searched via its charged currents (CC) interactions in the NOMAD detector: $\nu_\tau + N \rightarrow \tau^- + X$. In the NOMAD experiment, tau will be recognized trough its following decays:

- $\tau^- \rightarrow e^- + \overline{\nu_e} + \nu_\tau$
- $\tau^- \rightarrow \mu^- + \overline{\nu_\mu} + \nu_\tau$
- $\tau^- \rightarrow \pi + \nu_\tau$
- $\tau^- \rightarrow \rho^-(\pi^-\pi^0) + \nu_\tau$

- $\tau^- \rightarrow (\pi^-\pi^-\pi^+) + n\pi^0 (n \geq 0) + \nu_\tau$

which amount to about 85% of the total branching fraction. The search method is based on the kinematical and topological criteria. In the ν_τ events the escaping neutrinos are reflected in the imbalance of the event transverse momenta (p_T) and tau decay products have in average larger (p_T) than the background. This kind of analysis requires the excellent charged lepton identification (e and μ) and the precise measurement of the transverse momentum imbalance.

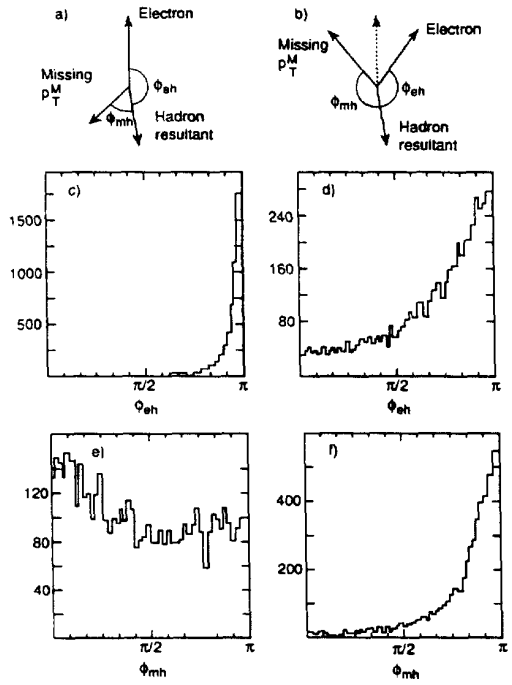

Figure 2: *Definition of the kinematical variables ϕ_{eh} and ϕ_{eh} for a) ν_e CC b) $\nu_\tau CC, \tau \rightarrow e$. Distributions of ϕ_{eh} and ϕ_{mh} for (c),(e) the background and (d),(f) the signal.*

As a example of kinematical cuts consider the electron channel : $\tau^- \rightarrow e^- + \overline{\nu_e} + \nu_\tau$. A major background for this τ decay mode is caused by CC interactions of the ν_e component of the beam (1%). This background is rejected considering the angles between the electron and the resultant hadronic vector ϕ_{eh} and between the missing p_T and the resultant hadronic vector ϕ_{mh}, in the transverse plane perpendicular to the beam direction (Fig. 2 (a,b)). For the background, since electron and hadrons are only participants in the reaction, the angle ϕ_{eh} will be sharply peaked at π (Fig. 2 (c)). The missing p_T in the ν_e CC interaction arises either from the missed neutral particles (n,K_L^0), which contribute with $\phi_{mh} \sim 0$, or from the mismeasurements which contribute with a flat distribution in ϕ_{mh} (Fig. 2 (e)). In the ν_τ event, the electron comes from the tau decay together with 2 neutrinos and will not necessarily be back-to-back with the hadron vector (Fig. 2 (d)). Missing p_T arises from the two neutrinos and is therefore centered on the tau direction, resulting in the ϕ_{mh} peak near π (Fig. 2 (f)). The ϕ_{mh} and ϕ_{eh} distributions are quite different for the signal and the background. The similar distributions are used in the muonic and hadronic chanels [1]. For the $\nu_\mu - \nu_\tau$ oscillations occuring just bellow the current limit on $sin^2(2\Theta) = 5 \times 10^{-3}$ for large Δm^2 one would expect 78 signal events over background of 7 events in the leptonic modes.

3 The NOMAD detector

The NOMAD detector (Fig. 3) was designed in order to provide an excellent electron identification and an accurate determination of the total transverse momentum in the event. Most of the detector components are located in a horizontal 0.4 T dipole magnetic field, perpendicular to the beam axis over the volume of $3.6 \times 3.5 \times 7.0 m^3$. It consists of following subdetectors ordered along the beam direction:

- the veto counters
- the forward calorimeter
- the drift chambers making an active target
- the trigger planes
- the transition radiation detector
- the preshower
- the electromagnetic calorimeter
- the hadronic calorimeter
- the muon chambers

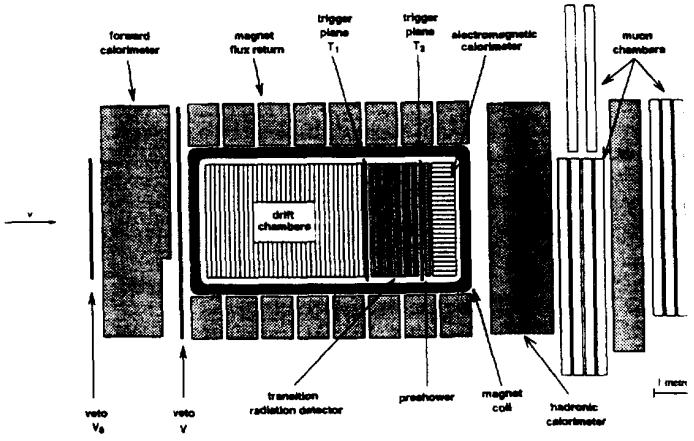

Figure 3: *A shematic sideview of the NOMAD detector.*

Charged particles produced in the neutrino interactions are measured in the drift chambers that play a role of fiducial target. The transition radiation detector provides the electon identification with the rejection of the pions better than 10^3 (90% electron efficiency). The electromagnetic calorimeter, completed with the preshower, measures electron and photons energies and improves the electron identification. The hadronic calorimeter [3] improves the mesurement of the hadronical system in the neutrino interactions, reducing the background that could arise from missed neutral hadrons. The muon identification is provided by the system of drift chambers placed behind the hadronic calorimeter.

3.1 The Forward Calorimeter

The Forward Calorimeter measures the energy and centroid of the hadronic showers in the neutrino interaction occuring in the detector support pillar. Since the FCAL target mass (17.7 t) produces about 10 times the rate of neutrino interactions in the active target, it will allow studies of multimuon physics and a search for heavy neutrinos.
The forward calorimeter instruments the central region of the detector support pillar. It consists of iron plates, separated by scintillators and corresponds to 5 nuclear interaction lenghts.

3.2 The Veto Counters

The veto system covers an area of $5 \times 5\ m^3$ at the upstream end of the NOMAD detector (Fig. 3). It consists of 59 scintillation counters arranged to provide the optimal rejection of the incoming charged particules produced upstream of NOMAD or inside the iron detector support. A set of 10 scintillation counters (denoted V_8) of total area $2.5m^2$, mounted in front face of the detector support pillar, form the veto for the forward calorimeter.

3.3 The Drift Chambers

The drift chambers provide at the same time the target material and the tracking of the particles. It implies that the drift chamber walls should be as heavy as possible to provide the neccesary statistics of neutrino interactions and as light as possible in order to minimize the multiple scattering and the electron degradation. In order to minimize the total number of radiation lenghts for a given target mass, the chambers are made of low density , low Z Aramid fibre honeycomb panels sandwiched between two Kevlar-epoxy layers. The honeycomb structure offers the mechanical rigidity and flatness over the surface of approximately $3 \times 3m^2$ that fills most of the avalible space inside tha coil. Each drift chamber consist of three planes of sense wires with stereo angles of $-5°, 0°$, and $+5°$ with respect to the magnetic field direction. The totality of 49 chambers is mounted in 11 modules each comprising 4 chambers, in the target part of the detector plus 5 individual chambers in the TRD region.
The fiducial mass of the chambers totals 2.4 tons. Each chamber corresponds to 0.02 radiation lenghts and there is never more than 0.01 radiation lenghts between two consecutive measurements. The totality of drift chambers does not exceed one radiation lenght.
The spatial resolution of the drift chambers is $\sigma = 150\mu m$ in the drift direction. With the stereo angles, the resolution along the wires (perpendicular to the bending plane) is 1mm. The momentum measurement resolution is about 5% for the charged hadrons and muons of energy 1 GeV. For the electron the momentum resolution is worsen because of the bremsstrahlung process and the information combined with the electromagnetic calorimeter is used to measure the electron energies.

3.4 The Trigger Counters

The main trigger is provided by two trigger planes T1 and T2, one located behind the active target and another behind the TRD. Each plane covers a fiducial area of $2.80 \times 2.86m^2$ and consists of 2 hodoscopes of 16 scintillation counters each. The scintillators are 5 mm thick and read out on one side.

3.5 The Transition Radiation Detector

The TRD provides a rejection factor for electrons over pions better than 10^3 for the particles of incident energy above 2 GeV. The high electron/pion separation is required in order to eliminate the background from about 10^4 isolated charged pions produced in neutral current events that survive the kinematical cuts. The total rejection factor of 10^5 is obtained by the combination of the TRD and the electromagnetic calorimeter.
In order to achive such a high rejection, the TRD consists of 9 individual modules. Each module includes a radiator by which the transition radiation is produced, followed by an x-ray detection plane. Five drift chambers are embedded between the TRD modules in order to improve the momentum mesurement and to provide the precise extrapolation of the tracks to the calorimeter front face.

The TRD was designed according to the several experimental constraints: the large detection area of $3 \times 3m^2$, small amount of material in order to keep the distance between two consecutive mesurements inferior to 0.02 radiation lenghts, limited space inside the magnet coil. Each TRD radiator consists of 315 polypropilene foils, $15\mu m$ thick, separated by a $250\mu m$ air gaps. The few emitted photons in the KeV energy range are absorbed in the plane of 176 straw tubes. Each straw tube is 3 m high with a diameter of 16 mm. The straws are made of mylar ribbon and filled with the mixture

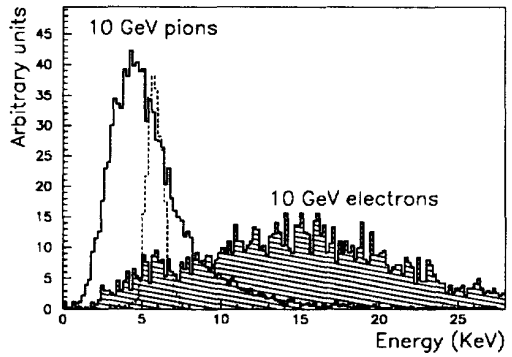

Figure 4: *Response of one TRD module to 10 GeV pions (solid line) and electrons(hashed). Dashed line shows the Fe^{55} calibration source*

Xe(80%)-methane(20%). About 70% of produced photons are absorbed in the first straw plane crossed. The energy calibration is obtained by Fe^{55} sources (5.86 KeV photons) deposited on the mylar ribbon at the middle of the each TRD plane.
Figure. 4 shows the response of the one module prototype to 10 GeV electrons and pions as measured in a test beam. The preliminary studie show that the expected rejection factor can be obtained with an efficiency on electrons of 90%.

3.6 The Preshower Detector

The preshower detector is located just in front of the electromagnetic calorimeter. It consists of two arrays of proportional tubes(286 horizontal and 288 vertical) preceeded by a 9 mm (1.6 X_0) lead-antimony converter. The tubes are made of extruded aluminium, with the square cross section of $9 \times 9mm^2$. The gas mixture is 80% Ar -20 % CO2.
Combined with the electromagnetic calorimeter, the preshower provides the electron identification with the rejection factor over pions better than 1000.
Because of its small granularity, compared to the electromagnetic towers, the preshower is also used to localize the the impact point of particles on the front face of the calorimeter and to disentagle the overlappings.

3.7 The Electromagnetic Calorimeter

The electromagnetic calorimeter measures the energy and the position of the electromagnetic showers for the electrons and photons with energies rangigng from about 100 MeV up to 100 GeV. The calorimeter consists of 875 lead-glass Cerenkov counters, 19 X_0 deep with a rectangular cross-section of $79 \times 112mm^2$ and total area of about $2.8 \times 2.8m^2$. The direction of B=0.4T magnetic field is perpendicular to the counter axis. The collection of the Cherenkov light is provided by the phototetrodes that operate in the magnetic field. The axes of the photo-tetrodes are at an angle of 45° to the magnetic field , limiting the reduction of the signal caused by the field to 20 %. Each lead glass counter has two monitoring LEDs glued close to the tetrode. Additional monitoring information is provided by the muon triggers. The overall variation of the muon signal in the FCAL after one year of operation is smaller than 4.
The mesured energy resolution in the range 10-80 GeV is : $\sigma(E)/E = 0.03/\sqrt{E} + 1\%$. The linearity of the response is within $\pm 0.2\%$.
When the calorimeter is used alone, it provides a charged pion rejection of about 100 for the electron efficiency of 90 %. Combined with preshower, it can achieve an electron-pion separation of 10^3.
The fast signal, with the resolution of a few ns for energy depositions larger than 1 GeV, allows using the ECAL at the trigger level.

3.8 The Hadronic Calorimeter

The hadronic calorimeter measures the energy and the position of the hadrons. It detects neutral hadrons (neutrons and K_L's) that deposit only the fraction of their energy in the electromagnetic calorimeter and disentangle the overlapping electromagnetic and hadronic particles. Iron absorber of the HCAL already existed since the magnet, used previously by the UA1, was instrumented as the hadronic calorimeter in that experiment. The HCAL consisits of 18 modules stacked up vertically covering an active area of $3.6 \times 3.6m^2$. Each module is composed of 11 planes of scintillators and corresponds to 3.1 interaction lenght λ in addition to 2.2λ provided by the electromagnetic calorimeter and magnet coil.
The arrangement of the ECAL followed by the coil follows by the HCAL is expected to provides an energy resolution of $120\%/\sqrt{E}$ (E in GeV) and a position resolution is estimated to be about $19cm/\sqrt{E}$.

3.9 The Muon Chambers

The muon identification is performed by 10 drift chambers situated outside the magnet. The chambers are arranged in 5 modules (pairs of 2 chambers) for track segment reconstruction. The first muon chamber consisits of three modules and is places just behind the haronic calorimeter that provides the muon filter. It is followed by an 80 cm thick iron absorber and a second muon station. Each chamber has an active area of $3.75 \times 5.55m^2$ with two planes of sense wires in the horizontal and two in the vertical direction. The chambers operate with an Argon/Ethane (80%/20%) mixture.
The average position resolution of hits is 400 μm in both drift directions. The overall measured efficiency for the reconstruction of the track segments is 97%.

3.10 Triggers and Data Acquisition

During of the SPS machine cycle of 14.4 s the neutrinos are produced in two 6 ms long spills separated by 2.4 s. The proton intensity is about 1×10^3 p.o.t/spill. Between two neutrino spills, the NOMAD detector collects the muons originating from secondaries produced in fixed target and beam facilities in the West Area. The time left is used for the calibration.

The NOMAD detectors provides several triggers in order to study the interactions occuring at the several parts of the detectors. The main trigger $\overline{V}T_1T_2$ is optimized for interactions in the active target since the trough-going muons are supressed by the veto counter V. The FCAL trigger $\overline{V_8}$ selects the interactions in the FCAL requiring an energy deposition corresponding to at least 3 minimum ionizing particles. The ECAL trigger $\overline{V}ECAL$ is implemented for the interactions occuring in the ECAL.

4 Data Collection

NOMAD started with data taking in April 1994. During the 1994 run the SPS delivered an integrated intensity of 8×10^{18} pot. that corresponds to the 30% of the total statistics requested for two years of data taking. Since only the 3 DC modules were present in the target region, an additional inactive target (1.6 t of polyethylene) was placed in front of the DC modules in order to enhance the rate of neutrino interactons. About 200 000 neutrino interactions at the fiducial volume and in the dummy target were recorded and analysed. This statistics allowed to demonstrate the performance of the different subdetectors and to study some general properties of the neutrino events.

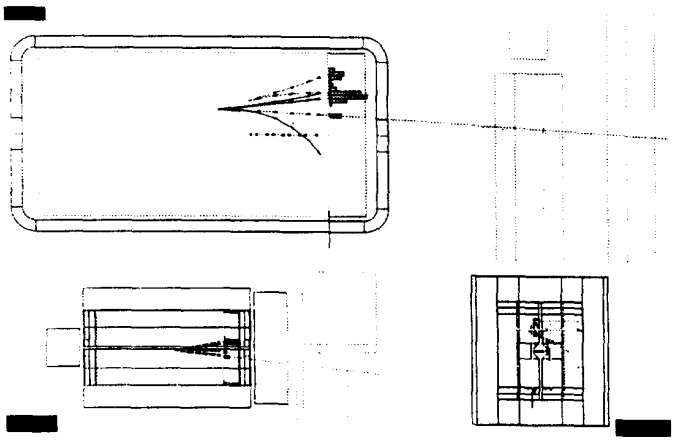

Figure 5: *A reconstructed ν_μ CC candidate from the 1995 run. Side, top and front view.*

Data taking was resumed in April 1995 with few DC moduled but without the inactive target. The detector was completed in the August with all 11 DC modules in the target region and the run continues until mid-October. The integrated SPS intensity (as to September 24th 1995) is 1.1×10^{19} pot. Fig. 5 shows a fully reconstructed ν_μ CC interaction in the active target recorded during the 1995 run.

5 Preliminary studies

A sample of 100 000 neutrino events recorded in July 1994 was used to study the electron and the muon signal. In order to select the events originating from the inactive target and reject those in the magnet coil, the detector support (now FCAL) and the magnet return yoke, we used the information on the vertex position reconstructed by the TRD in the nonbending plane. The detecor reponse was simulated for the interactions both in the inactive target and the surrounding materials using LEPTO [7] and GEANT [8].

In the muon analysis we extrapolate reconstructed drift chamber tracks trough the calorimeter and the iron absorber to the two muon chambers. The track is considered to be a muon candidate if it matches a track segment reconstructed in either of the two muon stations. The muon momentum is evaluated by the central drift chambers tracks. The resulting measured inclusive muon momentum distribution shown in Fig. 6 agrees well with the Monte-Carlo prediciton for $p > 5$ GeV (muon identification in the treshold region is still under study). As expected, the sample is dominated by the negative muons from the ν_μ CC events.

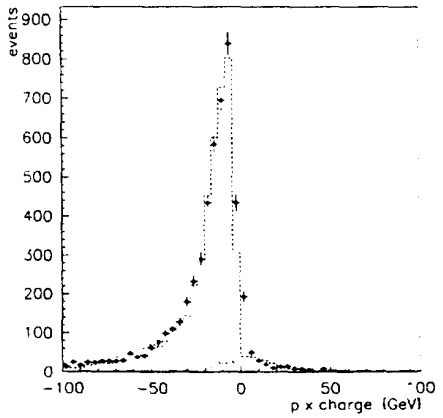

Figure 6: *Distribution of momentum times charge for identified muons originating from the inactive target (1994 run) compared to the Monte Carlo prediction. The dotted line indicates the contribution of events from the magnet coil and return yoke*

Resulting ν_μ CC sample was used the study other

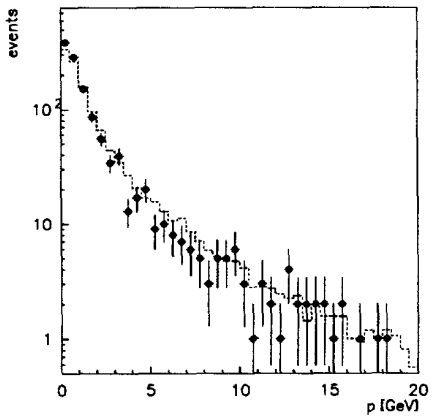

Figure 7: *Momentum distribution of drfit chamber hadron tracks (see text). The measured data points are compared to the Monte Carlo prediction (dashed line).*

charged tracks in the interaction excluding the one identified as muon. This concernes the charged hadrons and electron conversions. The momentum distribution of these tracks (here defined simply as hadrons) and the track multiplicity are shown in Fig. 7 and Fig. 8. The reasonable agreement with the predictions is achieved.

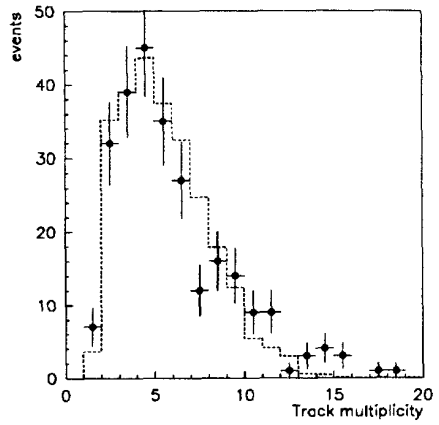

Figure 8: *Drift Chamber Hadron track multiplicity. (see text). The measured data points are compared to the Monte Carlo prediction (dashed line).*

To study the electron signal we used several criteria based on the response of different subdetectors. The electrons originate mainly from the photon conversions and π^0 Dalitz decays in the ν_μ CC and NC interaction. The challenge is to search for the evidence of the primary electrons that come from the CC interactions of ν_e which corresponds to 1% of the neutrino flux. An

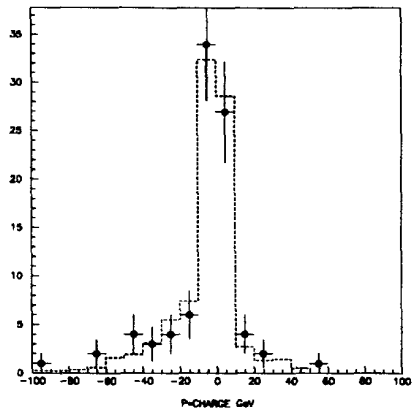

Figure 9: *Distribution of momentum times charge for identified electrons originating either from the assymetric photon conversions or from the ν_e CC interactions.(see text). The measured data points are compared to the Monte Carlo prediction (dashed line).*

electron(positron) candidate is selected in the following way: a) the energy deposition of the particle in the preshower should be greater than one of the 8 minimum ionizing particles b) the momentum measured in the drift chambers should be compatible with the energy measured in the electromagnetic calorimeter c) as to the TRD, the cut imposed on the maximum likelyhood function of the detector response was adjusted in order to provide an efficiency of 90% on a simulated electron sample. In order to reduce the number of secondary electrons in the resulting sample we impose the criteria on the lowest invariant electron-positron and electron-photon invariant mass. The momentum distribution of the remining cuts in shown in the Fig 9. The $\pm$ charge assymetry due to the ν_e CC interactions is well reproduced in the data.

6 Conclusion

The NOMAD experiment will explore new regions of neutrino mixing parameters for the cosmiolgically prefered ν_μ mass region. The NOMAD detector has been completed and is funnctioning well. The experiment will continue with the data taking until the end of 1997.

Acknowledgments

I would like to thank the organizers for a pleasant and stimulating conference.

References

[1] NOMAD Collab., CERN-SPSLC/91-21, CERN-SPSLC/91-48, CERN-SPSLC/91-53, CERN-SPSLC/93-19, CERN-SPSLC/94-28.

[2] CHORUS Collab., CERN-SPSC/90-42 (1990);M. de Jong *et al.*, CHORUS Collab., CERN-PPE/93-131.

[3] NOMAD Collab., CERN-SPSLC/93-31.

[4] N. Uschida *et al.*, Phys. Rev. Lett. 57 (19986) 2897.

[5] F. Dydak *et al.*, CDHS Collab., Phys. Lett. B134 (1984) 281.

[6] M. Gruwe *e al.*, CHARM-II Collab., Phys. Lett. B309 (1993) 463.

[7] "The LUND MC for Deep Inelastic Lepton-Nucleon Scattering, LEPTO 6.2",Physics at HERA, October 1991; T.Sjostrand,JETSET,Computer Physics Commun. 43 (1987) 367.

[8] GEANT 3.21, CERN Program Library Long Writeup W5031.